RSC Advances

ROYAL SOCIETY OF CHEMISTRY

www.rsc.org/advances

RSC Advances

ARTICLE

Cyclopentadienyl iron dicarbonyl ($CpFe(CO)_2$) derivatives as apoptosis-inducing agents

Received 00th January 20xx,
Accepted 00th January 20xx

DOI: 10.1039/x0xx00000x

www.rsc.org/

H.T. Poh,[a] P. C. Ho,[b] and W. Y. Fan[a]

Iron has been found to serve multiple purposes besides being an oxygen carrier. Of particular note is the generation of deletrious free radicals which can lead to the formation of tumours. However, in this work, we have found that cyclopentadienyl iron carbonyl complexes $CpFe(CO)_2X$ (X=halide, NCS, BF_4^- and $CpFe(CO)_2$) can induce apoptosis in breast cancer and HeLa cell lines. Normal cells are however unaffected. A detailed study on $CpFe(CO)_2I$ shows that the complex is metabolic-stable and easily permeable across a lipid barrier. Prelimiary Investigations into the mode of action suggest that a Fenton-type reaction caused by $CpFe(CO)_2$ complexes may be related to cell death.

Introduction

The success of cisplatin in testicular cancer treatment has led to much research interest in the discovery of organometallic anti-cancer compounds[1, 2] such as arene ruthenium[3-7], ferrocene derivatives[8-10,11] and metal carbene[12-14] complexes. Although not as prevalent, metal carbonyl complexes have also been featured as anti-cancer compounds since the first demonstration of cytotoxicity by alkyne hexacarbonyldicobalt species.[15-18] An iron carbonyl diene nucleoside complex has been shown to induce apoptosis in cancer cells[19, 20] while rhenium carbonyl tamoxifen complexes bind strongly to estradiol receptor sites in breast cancer cells.[21, 22] Osmium carbonyl clusters[23] have been used as a new class of apoptosis-inducing agents while an iron dithiocarbamate carbonyl complex used as a CO-releasing molecule (CORM) can also exhibit anti-cancer activity.[24] Manganese carbonyl N-heterocycles showed photo-induced cytotoxicity[25-27] and half-sandwich cymantrene peptides conjugates are potential candidates in anticancer chemotherapy[28-30]. Our motivation in using inexpensive iron carbonyls as anti-cancer agents came during *in vitro* testing of organic and inorganic isothiocyanates on ER- (estrogen receptor negative) breast carcinoma cancer cells (MDA-MB-231). We discovered that cyclopentadienyl iron dicarbonyl isothiocyanate $CpFe(CO)_2NCS$ demonstrated more potent cytotoxicity towards these cells, compared to sulforaphane, an organic isothiocyanate found in cruciferous vegetables.[31, 32] Importantly, the normal cells are unharmed by the iron complexes. This promising result initiated a series of expe riments to evaluate the cytotoxicity of $CpFe(CO)_2X$ class of complexes on MDA-MB-231 cells as well as the more widely researched HeLa cell-line. Indeed, our results have suggested that even without the isothiocyanate functionality, these metal complexes are still cytotoxic down to IC_{50} (inhibitory concentration) values of a few μM while leaving normal cells intact.

Previous published literature work have pointed out that iron while is best known for its role in the formation of the oxygen carrier haemoglobin, it is also involved in a wide range of biological processes such as metabolism, cell replication and detoxification[33]. Chemically, iron exists in solution as the hydrated Fe^{2+} and Fe^{3+} ions, and these species undergo facile electron transfer and acid-base reactions. This redox capability allows iron to partake in enzymatic reaction, but at the same time also enables it to participate in potentially deleterious biological events such as free radicals generation. The simplest of such events is the Fenton reaction which generates two reactive oxygen species – superoxide ($O_2^{-\bullet}$) and hydroxyl ($OH^{\bullet}$) radical from the reactions of the iron cations with hydrogen peroxide, a major by-product of aerobic respiration.

The essential yet toxic dual property of iron necessitates a deeper understanding of how iron works in a biological system. The recent discovery of new proteins that are involved in iron metabolism[34] have now greatly facilitated our understanding of the dual traits of iron in our body. For example, newly identified iron efflux pumps[35], iron regulators, oxidases and reductases[36-38] have offered scientists a new look at how tumours cells influence and impact normal iron metabolism. These studies not only provide valuable knowledge on the relationship between iron and cancer, they have also opened up the possibility of a new class of iron-based therapeutics.

[a] *Department of Chemistry*
3 Science Drive 3, National University of Singapore, Kent Ridge, Singapore 117543
[b] *Department of Pharmacy*
18 Science Drive 4, National University of Singapore, Kent Ridge, Singapore 117543

† *Footnotes relating to the title and/or authors should appear here.*

Electronic Supplementary Information (ESI) available: [details of any supplementary information available should be included here]. See DOI: 10.1039/x0xx00000x

These new knowledge on iron as potential anti-cancer agents have motivated us to pursue the use of our iron half sandwich complexes as new candidates in the research for anti-cancer treatments.

Results and discussion

Chemistry. Seven iron complexes of formula $CpFe(CO)_2X$ (**1** to **7**, Scheme 1) and for comparison purposes, three metal carbonyl dimers $[CpMo(CO)_3]_2$ (**8**), $Re_2(CO)_{10}$ (**9**) and $Mn_2(CO)_{10}$ (**10**), have been tested for cytotoxicity against MDA-MB-231 breast cancer cells and HeLa cervical cancer cells. Complexes **1**, **2**, **4**, **5** and **6** were prepared according to slightly-modified literature methods[39, 40] while **3**, **7**, **8**, **9** and **10** were commercially available.

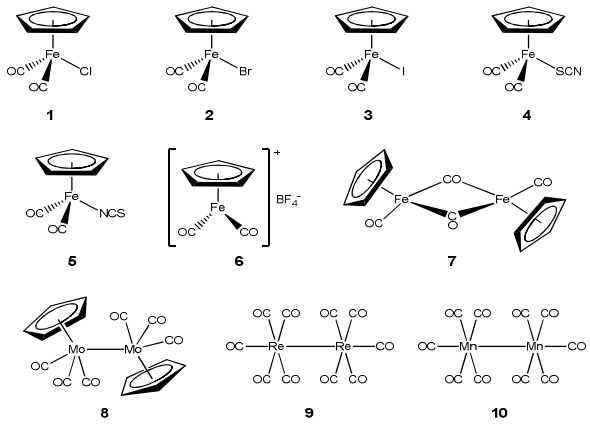

Scheme 1. Structures of the ten metal carbonyl complexes used.

To complete the structural characterization of the complexes in Scheme 1, the X-ray single crystal structures of yellow $CpFe(CO)_2NCS$ (**5**) and its red isomer, $CpFe(CO)_2SCN$ (**4**) were obtained (Figure 1). We note that the crystal data of $CpFe(CO)_2NCS$ (**5**) have been published in 1980[41], but our crystal data obtained here have a much better R/wR value and hence they are being reported again. The Fe-NCS moiety in $CpFe(CO)_2NCS$ (**5**) is close to linearity with a Fe-N-C angle of 178.90(3)^o and with a short N≡C bond of 1.159(5) Å adopting triple bond character. In contrast, a bent Fe-S-CN angle of 100.96(17)^o due to lone pair repulsion is determined in $CpFe(CO)_2SCN$ (**4**) instead, with a C≡N bond length of 1.163(7) Å. The C≡N bond lengths in both isomers are similar to those found in organic thiocyanates and isothiocyanates. The more efficient π-backbonding from NCS to the metal centre in the linear Fe-NCS fragment of $CpFe(CO)_2NCS$ also leads to its slightly higher υ_{CO} values compare to those of $CpFe(CO)_2SCN$.

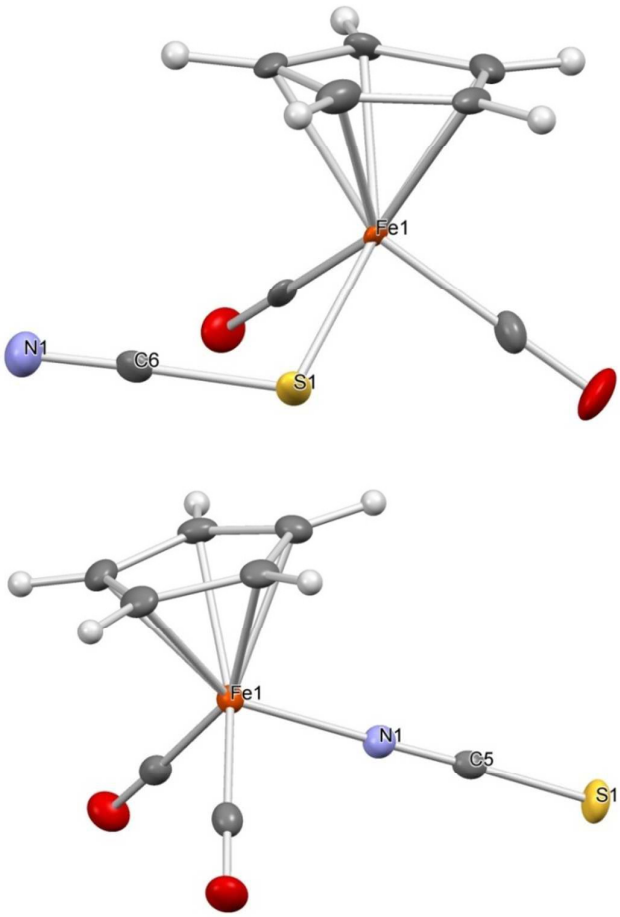

Figure 1. ORTEP diagram of (top) $CpFe(CO)_2SCN$ (**4**) and (bottom) $CpFe(CO)_2NCS$ (**5**) (thermal elipsoids at 50% probability).

Biological Evaluation. The IC_{50} values for **1** to **10** evaluated against ER- breast carcinoma cancer cells (MDA-MB-231) and HeLa cervical cancer cell line are shown in Table 1 (see supplementary information 1 and 2, for the respective dose-response curves). All the iron complexes **1** to **7** showed cytotoxicity towards the cancer cells with IC_{50} values ranging from 3.0 μM to 17.3 μM, with **3** being the most potent over a 24-hour incubation period. The presence of the SCN/NCS group in **4** and **5** does not appear to impart additional cytotoxicity as compared to the rest of the $CpFe(CO)_2$ derivatives. In contrast, dimers **8, 9** and **10** do not show appreciable cytotoxicity. Remarkably, all the complexes are not cytotoxic towards the corresponding normal mammary epithelial cells MCF-10A and two other normal cell lines, TAMH (Transforming growth factor- alpha mouse hepatocyte) and HL-1 (Mouse cardiomyocyte derived from AT-1 mouse atrial cardiomyocyte tumor lineage).[42] IC_{50} values could not be determined since the normal cell viabilities over the tested concentration range remain close to 100%. Although the IC_{50} values for cancer cell cytotoxicity are not in the nM (nanomolar) range, the iron complexes induce only cancer cell death while leaving normal cells intact.

Table 1. Inhibition of cell proliferation by the metal carbonyls measured with MDA-MB-231 carcinoma breast cells and HeLa cervical cancer cells after 24 h incubation, as determined by MTS assay. *The IC50 values for the complexes tested on the three different normal cell lines (MCF-10A, TAMH, HL-1) are >200μM and hence are not reported.

[IC_{50}] / μM					
Complex	MDA-MB-231	HeLa	Complex	MDA-MB-231	HeLa
1	17.3 ± 1.3	18.3 ± 1.2	6	8.7 ± 1.1	9.0 ± 1.0
2	10.5 ± 1.2	13.7 ± 1.2	7	13.6 ± 1.2	15.5 ± 1.2
3	3.0 ± 1.1	6.7 ± 1.1	8	>200	>200
4	3.4 ± 1.1	7.0 ± 1.1	9	>200	>200
5	3.8 ± 1.1	8.0 ± 1.2	10	>200	>200

As complex **3** is highly effective against both forms of cancer cells inferred from the confocal and flow cytometry data, we have chosen this complex as the lead compound to further our investigations into cell death. The effect of **3** on the MDA and HeLa cancer cells can be observed by microscopic imaging (Figure 2). The cells were initially of regular shape with the cellular membranes clearly visible and defined. After treatment with complex **3**, cell blebbing was observed in which the cells became irregularly-shaped because of the decoupling of the cytoskeleton from the plasma membrane followed by eventual loss of cytoplasmic material. The nuclei were no longer visible and the cytoplasmic membranes were not clearly defined. This blebbing process is widely believed[43-45] to be an indicator of apoptosis.

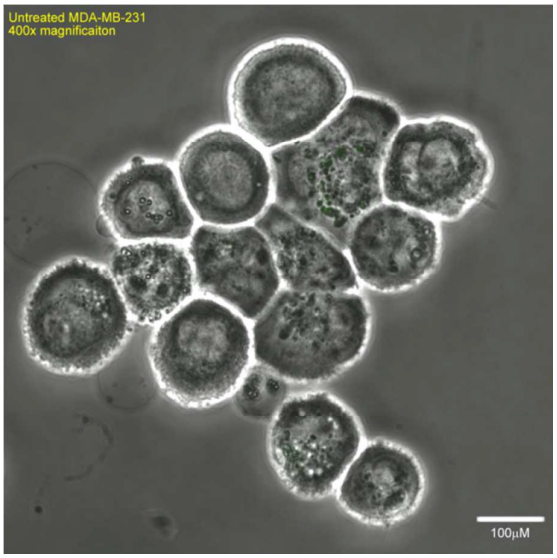

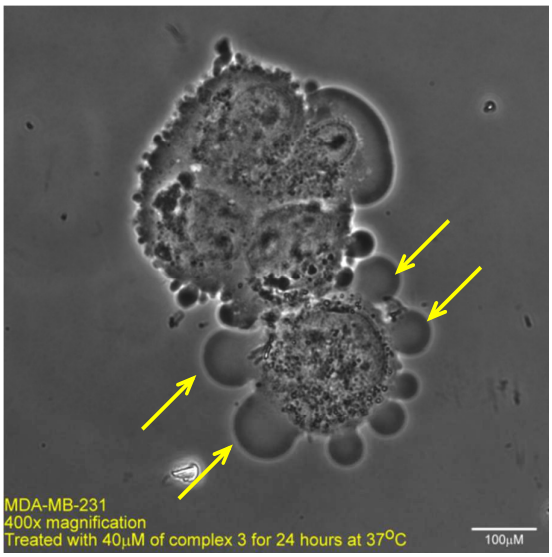

Figure 2. Bright field image at 400× magnification of MDA-MB-231 mammary cancer cells before and after treatment with 40μM of complex **3** for 24 hours at 37°C. The cells in both images have been trypsinized prior as they were the same samples used for flow cytometry. The untreated cells show clearly the presence of an intact cell membrane. The bottom image shows multiple blebs (indicated by arrows) on a cell which is characteristic of apoptosis.

This is further supported by flow cytometry data in Table 2 which indicated that the Annexin V-stained cells treated with 5 μM of complex **3**, **6** or **7** underwent early apoptosis (see supplementary information 3 and 4 for the flow cytometry dot blots). Increasing the dosage to 10 μM caused a larger proportion of the cells to proceed to late apoptosis phase (doubly-stained by propidium iodide and Annexin V). In addition, the same complexes showed no effect on normal mammary epithelial cell line MCF-10, which reinforces the cell viability data (see supplementary information 5 for the flow cytometry dot blots).

Confocal images taken with varying concentrations of **3** are illustrated in Figure 3. As observed, the Annexin V-stained cells also showed that the cell membranes have undergone blebbing with the presence of large swollen nuclei, which suggest that the cells are undergoing late apoptosis. We have also imaged the cells in the presence of **7** and similar observations in cell blebbing were noted.

Table 2. Flow cytometry data for MDA-MB-231 (top) and HeLa (bottom) at 0 μM, 5 μM and 10 μM for complexes **3**, **6** and **7**. The average of three independent runs is shown. Values are represented as percentages.

(Top)

	3			**6**			**7**		
	0 μM	**5μM**	**10μM**	**0μM**	**5μM**	**10μM**	**0μM**	**5μM**	**10μM**
Live cells	99.4	88.0	72.7	99.8	89.2	71.6	83.3	62.0	58.8
Early Apoptotic	0.2	10.2	19.2	0.1	9.2	21.1	0.3	31.4	18.6
Late Apoptotic	0.0	1.7	7.6	0.1	1.2	6.8	2.3	5.8	17.7

(Bottom)

	3			6			7		
	0 μM	5μM	10μM	0μM	5μM	10μM	0μM	5μM	10μM
Live cells	99.6	79.6	67.0	94.5	76.7	69.7	96.0	67.6	62.6
Early Apoptotic	0.2	16.1	12.7	1.8	14.5	18.9	1.9	21.2	22.7
Late Apoptotic	0.0	4.1	16.8	2.4	5.4	10.6	1.6	10.9	12.3

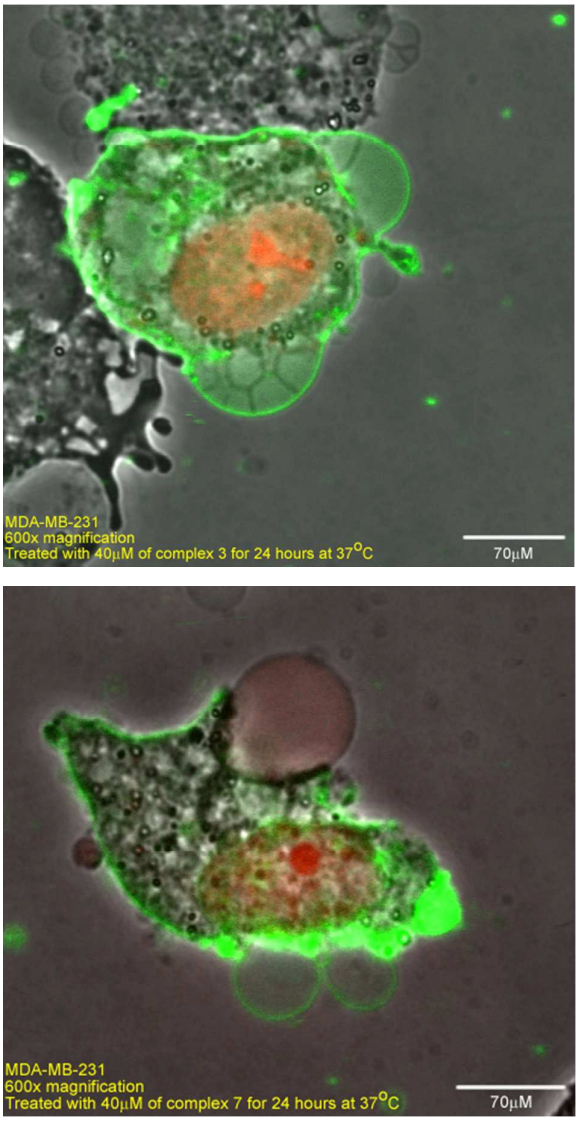

Figure 3. (top) Confocal image of MDA-MB-231 cells doubly stained with Annexin V Alexa Fluor 488 (green) and PI (red) taken at 600× magnification after treatment with 40μM of complex **3** for 24 hours at 37°C. The nucleus (red) is observed to be swollen together with the presence of blebbing (green) suggests that the cell is undergoing late apoptosis. (bottom) Confocal image of MDA-MB-231 cells doubly stained with Annexin V Alexa Fluor 488 and PI taken at 600× magnification after treatment with 40μM of complex **7** for 24 hours at 37°C. Blebbing is again observed together with a large swollen nucleus.

From the confocal images in Figure 4 taken over the same area, the effect of increasing the dosage of **3** also increased the number of cells undergoing early apoptosis, which are indicated by the Annexin-V stain (see supplementary information 6 and 7 for the complexes **4**, **5**, **6** and **7**). In the absence of **3**, no cell apoptosis was detected.

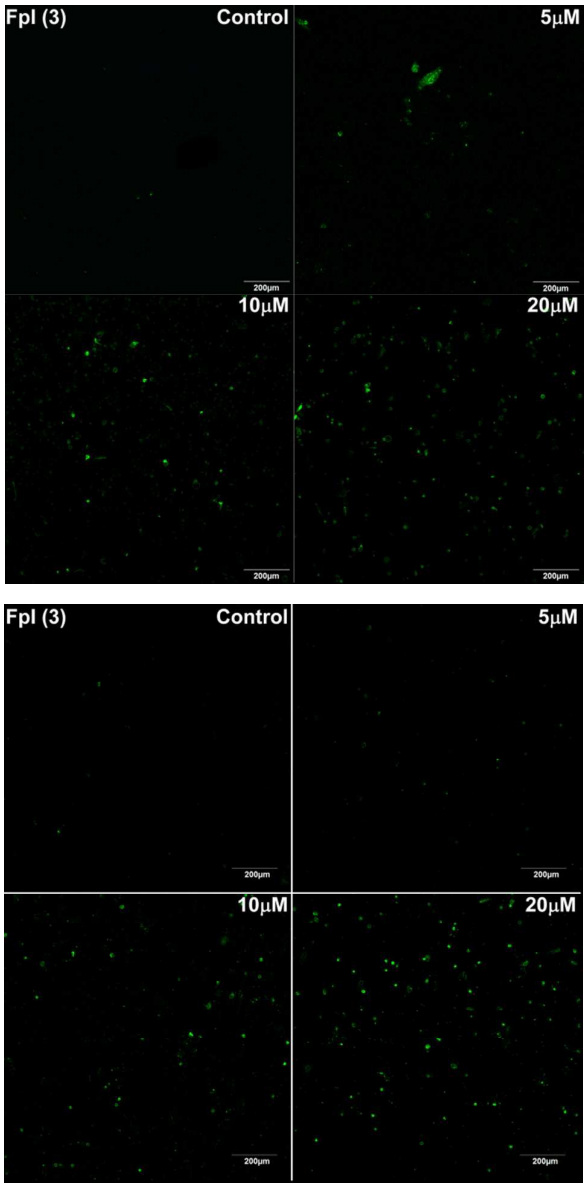

Figure 4. Confocal images of MDA-MB-231 (top) and HeLa (bottom) treated with 0 μM (control) 5 μM, 10 μM, 20 μM of **3** for 24 hours at 37°C Cells were stained with Annexin V (green) and PI (red).

Complex **3** and complex **7** have been used for further studies into their water-solubility, permeability across a membrane and metabolic stability. The solubilities of **3** and **7** in water have been determined to be 141 ± 20 μM and 31 ± 2 μM respectively. These values were determined by first dissolving weighed amounts of **3** and **7** with stirring in a known volume of

deionized water until the first sign of excess solids were seen at the bottom of the cuvette. The UV-vis absorbance was then monitored until it reached a constant value for at least an hour. The UV-vis spectra of the complexes in water and in hexane also appeared similar hence **3** and **7** should still be structurally intact without undergoing extensive dissociation in water.

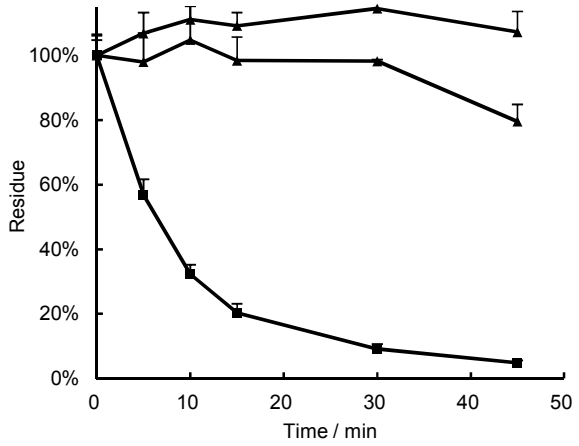

Figure 5. Metabolic stability studies of complex **3** in both MRLM (▲) and FRLM (•) versus a positive control, midazolam (■)

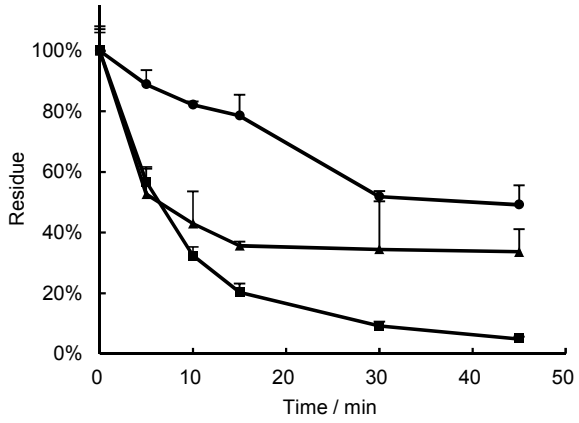

Figure 6. Metabolic stability studies of complex **7** in both MRLM (▲) and FRLM (•) versus a positive control, midazolam (■)

The *in vitro* metabolic stability of **3** and **7** was studied by assessing the percentage loss of the complexes over time in the presence of pooled male rat liver microsomes (MRLM) and female rat liver microsomes (FRLM) (Figures 5 and 6).[46] An estimate of the *in vitro* degradation half-life ($t_{1/2}$) and intrinsic clearance (CL_{int}) can be determined. Compare to midazolam, a compound which is rapidly metabolized, complex **3** is shown to be very metabolic-stable in rat liver microsomes. In contrast, **7** is very metabolic-unstable under the same conditions. It is metabolized to 40% in less than 15 min though the compound remains stable thereafter.

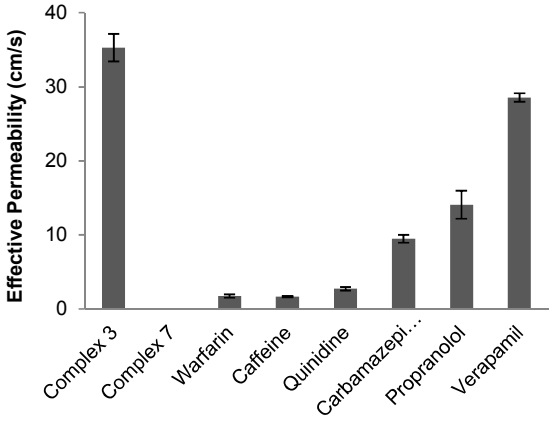

Figure 7. Permeability studies of complexes **3** and **7** using lecithin as the barrier, as compared against some established drugs after 6 hours of incubation. Similar results were obtained from the PAMPA studies made at 16 hours. Note also that the permeability of **7** is zero.

The effective permeability of these two complexes was determined by the parallel artificial membrane permeation assay (PAMPA) which is widely employed in the pharmaceutical industry to predict oral absorption potential of early drug candidates (Figure 7).[47-49] The PAMPA assay indicates that **3** has good permeability across lecithin as a lipid barrier after 6 hours of incubation. In fact the effective permeability of **3** is even higher than verapamil, a drug which already exhibits high permeability for the period of testing. In contrast, **7** does not show measurable permeability across lecithin.

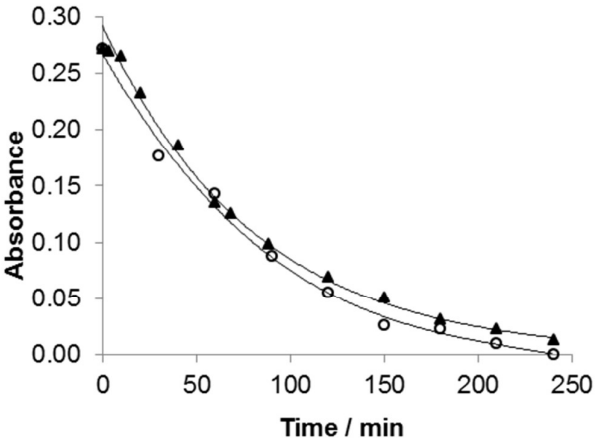

Figure 8. Decay of carbonyl stretching frequency of **3** and **7** upon reaction with 30% hydrogen peroxide. ○: **3** ; ▲: **7**

Chemical reactivity studies carried out on **3** and **7** showed that they do not react with natural amino acids such as glycine (control), lysine (amine), tyrosine (phenol), histidine

(imidazole), serine (aliphatic alcohol), methionine (sulfide) and cysteine (thiol) at 35 to 40°C over a period of 12 hours. This conclusion was derived from the monitoring of the CO infrared stretching signals of **3** and **7** after the addition of the respective amino acids in DMSO. In particular, this inactivity towards cysteine suggests that these iron complexes operate via a different mode of action in cellular growth inhibition contrary to organic isothiocyanates which target cysteine residues on the Keap1 protein.[50-52] Radical-mediated cell apoptosis pathways have also been considered, since the dimers **7** to **10** are well-known precursors to reactive mononuclear metal-centered radicals upon thermal or photochemical excitation.[53] The presence of such radicals in a cell environment could disrupt radical-dependent cell cycles. However the lack of cytotoxicity exhibited by **8**, **9** and **10** lends little support to a direct radical-mediated cell death. In addition, the role of **3** and **7** as CORMs is also unlikely. If CO release triggers cell death directly, all the tested metal carbonyls would have shown similar cytotoxicity effects.

The IC_{50} values listed in Table 1 suggests that cell death is brought about by the presence of the $CpFe(CO)_2$ moiety. Studies[54-56] have shown that there is an abundance of highly-oxidizing reactive oxygen species (ROS) in cancer cells, which promotes the Fenton reaction in which Fe^{2+} is oxidized to Fe^{3+}. The feasibility of this reaction was tested using hydrogen peroxide to represent an ROS. Indeed, the υ_{CO} IR absorbances of **3** and **7** showed a decrease against time, albeit at a much lower decomposition rate compare to $FeSO_4$, a typical iron salt used in the Fenton test (Figure 8). Upon completion of the reaction, a further chemical test with potassium thiocyanate turns the solution mixture red, indicating the presence of Fe^{3+}. Complexes **3** and **7** therefore are possible Fenton-type catalysts which might have disrupted ROS-mediated cell cycles leading to premature cancer cell death.[57] In contrast, the much lower ROS concentration present in normal cells may have mitigated the impact caused by the iron complexes.

Conclusions

In conclusion, we have shown that cyclopentadienyl iron carbonyl complexes are cytotoxic towards breast cancer cells but not against normal cells, with IC_{50} values of ranging from 3.0 μM to 17.3 μM. These complexes are structurally similar, each containing a $CpFe(CO)_2$ core with a differing functional group directly bonded to the iron center. With other metal carbonyls dimers, no significant cytotoxicity on the cancer cells was observed. As such, it is inferred that it is the $CpFe(CO)_2$ moiety that is largely responsible for the cytotoxic observations. The functional group on the iron does not appear to impart additional cytotoxicity to the complex as exemplified by the isothiocyanate complex. These half-sandwich iron complexes are inexpensive, either commercially available or easily prepared. In particular, $CpFe(CO)_2I$ is metabolic-stable and demonstrates good permeability across a lipid barrier and could be a potential candidate for future *in vivo* studies. While the mechanism of action remains to be elucidated, we believe that the pathway to cellular death may be associated with Fenton-like reactions caused by the $CpFe(CO)_2$ cation. We hope to stimulate interest in pursuing cyclopentadienyl iron carbonyl derivatives as potential anti-cancer therapeutic agents.

Experimental

General Procedures. All manipulations for chemical synthesis were carried out using standard Schlenk techniques under a nitrogen atmosphere. Photochemical experiments were conducted with a Legrand broadband lamp (350 – 800nm, 11W). All IR spectra were obtained with Shimadzu IR Prestige - 21 Fourier – transformed infrared spectrometer (1000 – 4000 cm^{-1}, 1 cm^{-1} resolution, 16 scans co–added for spectra averaging) using a 0.05mm path – length CaF_2 cell for liquid samples. Electrospray ionisation (ESI) was conducted using a Finnigan MAT LCQ spectrometer. Single crystal X-ray structural studies were performed on Bruker-AXS Smart Apex CCD Single-Crystal Diffractometers. Data were collected at 100(2)K using graphite-monochromated Mo K_α radiation (λ=0.71073Å). Data collection was evaluated using SMART CCD system.

Materials. Cyclopentadienyl iron dicarbonyl dimer $[CpFe(CO)_2]_2$, cyclopentadienyl dicarbonyl iodide $[CpFe(CO)_2I]$, cyclopentadienyl molybdenum tricarbonyl, $[CpMo(CO)_3]_2$, rhenium carbonyl $[Re_2(CO)_{10}]$, manganese carbonyl $[Mn_2(CO)_{10}]$, tetrachloromethane, dichloromethane, bromine, potassium thiocyanate, silver (I) tetrafluoroborate, ethanol, hexane, tetrahydrofuran and chloroform were purchased from Sigma-Aldrich. All chemicals were used without further purification.

Syntheses of $CpFe(CO)_2Cl$ (1), $CpFe(CO)_2Br$ (2) and $CpFe(CO)_2^+BF_4^-$ (6). $CpFe(CO)_2Cl$, $CpFe(CO)_2Br$ and $CpFe(CO)_2^+BF_4^-$ were synthesized according to literature methods[40]. $CpFe(CO)_2Cl$: υ_{CO} = 2057 cm^{-1}, 2012 cm^{-1} in chloroform; $CpFe(CO)_2Br$: υ_{CO} = 2045 cm^{-1}, 1999 cm^{-1} in ethyl acetate, $CpFe(CO)_2^+BF_4^-$: υ_{CO} = 2065 cm^{-1}, 2021 cm^{-1} in dichloromethane.

Syntheses of $CpFe(CO)_2SCN$ (4) and $CpFe(CO)_2NCS$ (5). Both isomers, $CpFe(CO)_2NCS$ and $CpFe(CO)_2SCN$, were obtained via a modified method[39]. Briefly, $[CpFe(CO)_2]_2$ dimer (35 mg, 0.1 mmol) was dissolved in absolute ethanol. 7 equivalents of potassium thiocyanate (70 mg, 0.72 mmol) and 0.6 ml of tetrafluoroboric acid were added under ambient conditions with vigorous agitation. The solvent was removed under reduced pressure after 1 hour and the two isomers were separated via column chromatography using silica as stationary phase and dichloromethane as the mobile phase. IR absorption bands conform to published literature. Crystals suitable for X-Ray analysis were grown from hexane. ($CpFe(CO)_2NCS$: υ_{CO} = 2067 cm^{-1}, 2023 cm^{-1} in dichloromethane, υ_{CN} = 2118 cm^{-1}; $CpFe(CO)_2SCN$: υ_{CO} = 2052 cm^{-1}, 2008 cm^{-1}, υ_{CN} = 2116 cm^{-1} in dichloromethane).

Reactions of 3 and 7 with H_2O_2. 4 mg of **3** (13 μmol) was dissolved in 2 ml of tetrahydrofuran (THF). 5 molar equivalents of aqueous hydrogen peroxide (30%) were then added and the mixture stirred under nitrogen. The changes in carbonyl absorption intensity of **3** at 2042 cm^{-1} were recorded at every 30 minutes interval for a total period of 4 hours until the signal becomes indistinguishable from background noise. The same procedure was carried out for the reaction between **7** (10 μmol, υ_{CO} band at 1790 cm^{-1}) and hydrogen peroxide in the same solvent.

Cell Culture and Drug Treatment. Experimental culture of the breast carcinoma MDA-MB-231, Human mammary epithelial cells MCF-10A, human cervical carcinoma cell HeLa and TGF-α mouse hepatocyte (TAMH) were obtained from the American Type Culture Collection (ATCC) and cultured in tissue culture flasks (Nunc Inc., Naperville, IL, USA). The HL-1 mouse cardiomyocyte was derived from AT-1 mouse atrial cardiomyocyte tumor lineage and obtained from the Department of Pharmacy, National University of Singapore. The cells were maintained in Dulbecco's modified Eagle's medium (DMEM, Grand Island, NY, USA) supplemented with 10% fetal bovine serum (FBS), 1% l-glutamate (GIBCO Laboratories), and 1% penicillin/streptomycin (GIBCO Laboratories) at 37°C in 5% CO_2 atmosphere. Phosphate buffered saline (PBS) was obtained from 1st Base.

Compounds **1** to **10** were dissolved in DMSO and serially diluted until the final concentration used for incubation were 0.01, 0.1, 1, 5, 10, 20, 40, 100 and 200μM. The treatment of the cells was performed by seeding the cells in growth medium at the same initial density. They were incubated for 24 hours to allow adhesion and growth before treatment (80% confluence). The cells were washed once with FBS-free medium and then serum starved for 12 hours before treatment with the various concentrations of the compounds in DMEM. Control cells were treated with 0.1% DMSO. All cell lines were treated in the same manner. All final DMSO concentrations are at 0.1%.

Annexin V and PI Staining for Flow Cytometry. The percentage of cells actively undergoing apoptosis was determined using Annexin-V Alexa Fluor 488 based immunofluorescence, as described previously[58]. Briefly, 10,000 cells were each seeded onto a 6-well dish and allowed to reach 80% confluence. The cells were then treated with **5** μM and **10** μM of **3**. After 24 hours, the cells were harvested and double-stained with Annexin-V and PI. The cells were then analyzed using BD LSRFortessa instrument running BD FACSDiva software. All experiments were performed in triplicates and yielded similar results.

Confocal Microscopy. High resolution images were obtained using Olympus Fluoview FV300 confocal laser scanning microscope at 400× and 600×. Cells were seeded on coverslips at a density of 10,000 cells per well in DMEM growth medium supplemented with 10% FBS and 1% penicillin/streptomycin and allowed to reach confluence over 24 h. They were then treated with the 5 μM, 10 μM, 20 μM, and 40 μM of **3** for 24 h. After treatment, the cells were washed with PBS, and stained with Annexin V and PI, then washed again with PBS and subsequently mounted onto a glass slide and examined and photographed. Apoptotic cells were defined based on the distribution of the Annexin V and PI stains. Early apoptotic cells were defined by Annexin V positive, PI negative. Necrotic and late apoptotic cells were defined by Annexin V and PI positive. Healthy cells were defined by Annexin V and PI negative.

Proliferation Assay. The anti-proliferation activity of the $CpFe(CO)_2X$ complexes were determined using MTS assay. Approximately 10,000 cells per well were seeded in a 96-well plate and allowed to adhere for approximately 24 hours at 37°C. The cells were then treated with varying concentrations of the complexes in media for another 24 hours and then left to incubate in a 37°C incubator with 5% CO_2. The final concentration of DMSO in the medium was 0.1% (v/v). Following treatment, 20 μL of MTS reagent was added and incubated for an additional 2 hours. The absorbance intensities at 490 nm were then measured and cell viabilities relative to the control (DMSO) were calculated. The IC_{50} values, which is defined as the concentration necessary to inhibit the growth of 50% of the cell population were then determined using Graphpad Prism version 5.0 by fitting the values on a dose-response curve (Cell viability vs log drug concentration). The experiments were performed in triplicates for each concentration and three independent experiments were performed.

Light Microscopy. 10,000 cells were each seeded onto a glass cover slips placed in a 6-well dish and allowed to reach 80% confluence in DMEM media. The cells were then treated with **20** μM and **40** μM of **3**. After 24 hours, the media was removed and the cells washed twice with PBS. The cover slips were then mounted onto glass slides and imaged under a light microscope.

Water Solubility and Stability Experiment. 0.100 mg portions of **3** and **7** was each separately added with stirring to 50 mL volume of deionized water until the first sign of excess solids were seen at the bottom of the cuvette. The experiment was then repeated three times to get an average value for the mass. The UV-vis absorbance was then subsequently monitored until it reached a constant value for at least an hour to evaluate the stability of the complex in water.

***In vitro* metabolic stability of 3 and 7 determination.** Pooled male and female rat liver microsomes were obtained from BD Gentest Corp. (Woburn, MA, USA). Milli-Q water (Millipore Corp., Milford, MA, USA) was used throughout the experiment. All other chemicals and reagents were of analytical grade and solvents were of HPLC grade. An Agilent 1100 series high performance-liquid chromatography system with diode array

detector (Agilent Technologies, Waldbronn, Germany) was employed for chemical analysis.

Chromatographic separation was performed on an Zorbax Eclipse Plus C18 column (2.1 X 100 mm, i.d., 3.5 µm, Agilent Technologies, Palo Alto, CA, USA) with a Security Guard Cartridge (3.0 X 4 mm, Agilent Technologies, Palo Alto, CA, USA) on isocratic elution using a mobile phase consisting of methanol–water (45:55, v/v) at a flow rate of 1.2 mL/min with UV detection at 262 nm. For sample analysis, a 20 µL sample injection was used. Phosphate buffer (100 mM, pH 7.4) containing 1 mM EDTA was prepared from 400 mM mono- and dibasic potassium phosphate stock solution. NADPH stock solutions (10 mM) in phosphate buffer were freshly prepared daily.

Liver microsomal incubations were conducted in triplicate. Incubation mixtures consisted of 7.5 µL of 20 mg/mL FRLM and MRLM (final: 0.3 mg microsome protein/mL), 2.5 µL of 600 µM of complexes **3** or **7** in acetonitrile (final: 3 µM), 440 µL of 0.1 M phosphate buffer (pH 7.4). The mixture was first shaken for 5 min for pre-incubation in a shaking water bath at 37^{O}C. Reaction was initiated by adding 50 µL of 10 mM NADPH to obtain a final concentration of 1mM NADPH in the mixture. The total volume of the reaction mixture was 500 µL. For metabolic stability studies, aliquots of 50 µL of the incubation sample mixture were collected at 0, 5, 10, 15, 30, and 45 min. After collection of samples, the reaction was terminated with 100 µL of chilled acetonitrile. The mixture was then centrifuged at 10,000 X g to remove the protein and the supernatant was subsequently applied to LC analysis.

Positive control (PC) samples were prepared as described above, except the test compound was replaced with the known P450 substrate (Midazolam, 3 µM). The samples were assayed for the degradation of midazolam to evaluate the adequacy of the experimental conditions for drug metabolism study. Negative control samples were also prepared as described above but without NADPH.

In the determination of the *in vitro* half-life ($T_{1/2}$), the peak areas of drug were converted to parent remaining percentages using the t = 0 peak area values as 100%. The remaining percentages of the candidate were plotted against the microsomal incubation time. Data points were determined from the average of three measurements with standard deviations as the error bars. The *in vitro* $T_{1/2}$ (in units of min) was calculated from the slope of the linear regression (k) of the natural logarithm of the parent remaining percentage versus incubation time according to the following formulae.

Equations:

$T_{1/2}$ = 0.693/k (min)

V (µL/mg) = Volume of incubation / amount of microsomal protein in the incubation (µl/mg)

$CL_{int,\ in\ vitro}$ = V x 0.693 / $T_{1/2}$ (µL/min/mg protein)

$CL_{int,\ app}$ = CL_{int} (45 mg microsomal protein/g of liver) (45 g of liver/kg body weight).

Permeability of complexes 3 and 7 determination. The effective permeabilities (P_e) of **3** and **7** were determined by the parallel artificial membrane permeation assay (PAMPA) which is widely employed in the pharmaceutical industry to predict oral absorption potential of early drug candidates. Permeability was assessed at pH 7.4 over 2 different permeation time, 6h and 16h, at ambient temperature. Caffeine, quinidine, verapamil, carbamazepine, warfarin, (±)-propranolol hydrochloride, L-α-phosphatidylcholine (lecithin) (Lyophilized powder from egg yolk) and **t**he phosphate buffer saline (PBS) solution were also obtained from Sigma Aldrich.

12 mM stock solution for each of the complexes **3** and **7** was prepared in DMSO. Calibrators were made in 1x PBS solution and diluted to give solutions of 120 µM, 60 µM, 30 µM, 15 µM, 7.5 µM, 3.75 µM, 1.875 µM, and 0.9375 µM. 250 µL of each calibrator solution was transferred to HPLC PP vials and analysed by HPLC-UV (254 nm). 50mM stock solution of each of the standards (caffeine, carbamazepine, quinidine, verapamil, propranolol, warfarin) was prepared in DMSO and diluted with 1xPBS to give standard calibrator solutions of 500 µM, 250 µM, 125 µM, 62.5 µM, 31.25 µM, 15.62 µM. The concentration of DMSO in each solution was kept at 1% (v/v). 250µL of each standard calibrator solution was transferred to separate wells in a 96-well flat bottom transparent UV plate. The UV/Vis absorbance of each well was read at λ max of the standard compound to give its calibration curve.

A 1% solution (w/v) of lecithin in dodecane was prepared and 5 µL of this 1% lecithin/dodecane solution was pipetted into the well of the donor plate. 12 mM stock solution of $CpFe(CO)_2I$ was prepared in DMSO. 10 µL of the 12 mM stock solution was diluted with 990 µL of 1x PBS buffer to give a 120 µM solution. The final concentration of DMSO in the solution is 1% (v/v). 300 µL of this solution was added to the well in the donor plate (with lecithin). 300 µL of 1x PBS buffer (containing 1% v/v DMSO) was added into the corresponding well in the acceptor plate. The donor plate was placed on top of the acceptor plate. The underside of the membrane in the donor plate must be in contact with the buffer in the acceptor well. The donor/acceptor plate unit was covered, placed in an air-tight container and agitated in an incubator (250rpm, 6 h) at temperature of 30.0^{o}C(± 2.5 ^{o}C). After this time, 250 µL/well of the donor and acceptor plates were transferred to separate HPLC PP vials. The concentration of analyte present in each sample were analyse by HPLC-UV (254 nm). The assay was repeated using a 2nd stock solution (12 mM) of $CpFe(CO)_2I$.

The Effective Permeability P_e was calculated from the equation below[49].

$$P_e = -2.303 \times \frac{V_A V_D}{V_A + V_D \times A \times t} \times \log\{1 - \frac{V_A + V_D}{V_D \times S} \times \frac{C_{A(t)}}{C_{D(0)}}$$

$$S = \left[\frac{V_A}{V_D} \times \frac{C_{A(t)}}{C_{D(0)}}\right] + \frac{C_{D(t)}}{C_{D(0)}}$$

where :
(i) C_A = concentration of test compound in acceptor well after period of incubation (6 h or 16 h).
(ii) $C_{D\,(0)}$ = concentrations of test compound at time 0
(iii) $C_{D\,(t)}$ = concentrations of test compound in donor wells after period of incubation (6 h or 16 h).
(iv) V_A= volume of acceptor well (0.3 cm^3)
(v) V_D = volume of donor well (0.3 cm^3)
(vi) A = filter area
(vii) t = permeation time (21600 s or 57600 s)
(viii) S = fraction of the sample remaining in the donor and the acceptor wells after permeation time

Chemical Reactivity Studies. The reaction of **3** and **7** with various amino acid substrates were evaluated as follow. 10 mg of **3** was first dissolved in 50 mL of DMSO. The initial infrared spectrum was obtained. Following that, 1 mole equivalent of the various amino acids was added separately to the solution of **3** and the solution warmed and maintained using a water bath at a temperature of 40°C. The IR bands were then monitored over 12 hours and conclusions were inferred from the changes to the infrared absorptions bands. The same procedure was applied to **7** to evaluate its chemical reactivity.

Acknowledgements

This work was supported by a NUS research grant (143-000-553-112). H.T.Poh acknowledges NUS-PGF for a scholarship.

Notes and references

‡ Footnotes relating to the main text should appear here. These might include comments relevant to but not central to the matter under discussion, limited experimental and spectral data, and crystallographic data.
§
§§
etc.

1 G. Gasser, I. Ott and N. Metzler-Nolte, *J. Med. Chem.*, 2011, **54**, 3-25.
2 C. Allardyce and P. Dyson, in *Bioorganometallic Chemistry*, ed. G. Simonneaux, Springer Berlin Heidelberg, 2006, vol. 17, ch. 1, pp. 177-210.
3 E. S. Antonarakis and A. Emadi, *Cancer Chemother. Pharmacol.*, 2010, **66**, 1-9.
4 A. Bergamo and G. Sava, *Dalton Trans.*, 2011, **40**, 7817-7823.
5 A. F. Peacock and P. J. Sadler, *Chem.Asian J.*, 2008, **3**, 1890-1899.
6 L. D. Dale, J. H. Tocher, T. M. Dyson, D. I. Edwards and D. A. Tocher, *Anticancer Drug Des*, 1992, **7**, 3-14.
7 P. J. Dyson and G. Sava, *Dalton Trans.*, 2006, 1929-1933.
8 A. Houlton, R. M. G. Roberts and J. Silver, *J. Organomet. Chem.*, 1991, **418**, 107-112.
9 P. Koepf-Maier and H. Koepf, *Chem. Rev.*, 1987, **87**, 1137-1152.
10 E. Neuse, *J. Inorg. Organomet. Polym. Mater.*, 2005, **15**, 3-31.
11 D. R. van Staveren and N. Metzler-Nolte, *Chem. Rev.*, 2004, **104**, 5931-5986.
12 J. L. Hickey, R. A. Ruhayel, P. J. Barnard, M. V. Baker, S. J. Berners-Price and A. Filipovska, *J. Am. Chem. Soc.*, 2008, **130**, 12570-12571.
13 I. Ott, *Coord. Chem. Rev.*, 2009, **253**, 1670-1681.
14 D. A. Medvetz, K. M. Hindi, M. J. Panzner, A. J. Ditto, Y. H. Yun and W. J. Youngs, *Met.-Based Drugs*, 2008, **2008**.
15 I. Ott, B. Kircher, R. Dembinski and R. Gust, *Expert Opin. Ther. Pat.*, 2008, **18**, 327-337.
16 I. Ott, K. Schmidt, B. Kircher, P. Schumacher, T. Wiglenda and R. Gust, *J. Med. Chem.*, 2005, **48**, 622-629.
17 M. A. Neukamm, A. Pinto and N. Metzler-Nolte, *Chem. Commun.*, 2008, 232-234.
18 G. Gasser, M. A. Neukamm, A. Ewers, O. Brosch, T. Weyhermüller and N. Metzler-Nolte, *Inorg. Chem.*, 2009, **48**, 3157-3166.
19 J. C. Franke, M. Plotz, A. Prokop, C. C. Geilen, H. G. Schmalz and J. Eberle, *Biochem. Pharmacol.*, 2010, **79**, 575-586.
20 D. Schlawe, A. Majdalani, J. Velcicky, E. Hessler, T. Wieder, A. Prokop and H. G. Schmalz, *Angew Chem Int Ed Engl*, 2004, **43**, 1731-1734.
21 S. Top, A. Vessieres, P. Pigeon, M. N. Rager, M. Huche, E. Salomon, C. Cabestaing, J. Vaissermann and G. Jaouen, *ChemBioChem*, 2004, **5**, 1104-1113.
22 G. Jaouen, S. Top, A. Vessieres, G. Leclercq and M. J. McGlinchey, *Curr. Med. Chem.*, 2004, **11**, 2505-2517.
23 K. V. Kong, W. K. Leong, S. P. Ng, T. H. Nguyen and L. H. Lim, *ChemMedChem*, 2008, **3**, 1269-1275.
24 L. Hewison, S. H. Crook, B. E. Mann, A. J. H. M. Meijer, H. Adams, P. Sawle and R. A. Motterlini, *Organometallics*, 2012, **31**, 5823-5834.
25 H. W. Peindy N'Dongo, I. Ott, R. Gust and U. Schatzschneider, *J. Organomet. Chem.*, 2009, **694**, 823-827.
26 J. Niesel, A. Pinto, H. W. Peindy N'Dongo, K. Merz, I. Ott, R. Gust and U. Schatzschneider, *Chem. Commun.*, 2008, 1798-1800.
27 I. Neundorf, J. Hoyer, K. Splith, R. Rennert, H. W. Peindy N'Dongo and U. Schatzschneider, *Chem. Commun.*, 2008, 5604-5606.
28 W. Hu, K. Splith, I. Neundorf, K. Merz and U. Schatzschneider, *J. Biol. Inorg. Chem.*, 2012, **17**, 175-185.
29 K. Splith, W. Hu, U. Schatzschneider, R. Gust, I. Ott, L. A. Onambele, A. Prokop and I. Neundorf, *Bioconjugate Chem.*, 2010, **21**, 1288-1296.
30 K. Splith, I. Neundorf, W. Hu, H. W. P. N'Dongo, V. Vasylyeva, K. Merz and U. Schatzschneider, *Dalton Trans.*, 2010, **39**, 2536-2545.

31 J. W. Fahey, Y. Zhang and P. Talalay, *Proc. Natl. Acad. Sci. U. S. A.*, 1997, **94**, 10367-10372.

32 P. Talalay, J. W. Fahey, Z. R. Healy, S. L. Wehage, A. L. Benedict, C. Min and A. T. Dinkova-Kostova, *Proc. Natl. Acad. Sci. U. S. A.*, 2007, **104**, 17500-17505.

33 R. Crichton, in *Iron Metabolism*, John Wiley & Sons, Ltd, 2009, ch2, pp. 17-58.

34 N. C. Andrews, *Blood*, 2008, **112**, 219-230.

35 E. Nemeth, M. S. Tuttle, J. Powelson, M. B. Vaughn, A. Donovan, D. M. Ward, T. Ganz and J. Kaplan, *Science*, 2004, **306**, 2090-2093.

36 S. A. Shoichet, A. T. Bäumer, D. Stamenkovic, H. Sauer, A. F. H. Pfeiffer, C. R. Kahn, D. Müller-Wieland, C. Richter and M. Ristow, *Hum. Mol. Genet.*, 2002, **11**, 815-821.

37 T. J. Schulz, R. Thierbach, A. Voigt, G. Drewes, B. Mietzner, P. Steinberg, A. F. H. Pfeiffer and M. Ristow, *J. Biol. Chem.*, 2006, **281**, 977-981.

38 R. Lill, B. Hoffmann, S. Molik, A. J. Pierik, N. Rietzschel, O. Stehling, M. A. Uzarska, H. Webert, C. Wilbrecht and U. Mühlenhoff, *Biochimica et Biophysica Acta (BBA) - Molecular Cell Research*, 2012, **1823**, 1491-1508.

39 T. E. Sloan and A. Wojcicki, *Inorg. Chem.*, 1968, **7**, 1268-1273.

40 B. M. Mattson and W. A. G. Graham, *Inorg. Chem.*, 1981, **20**, 3186-3189.

41 A. F. Berndt and K. W. Barnett, *J. Organomet. Chem.*, 1980, **184**, 211-219.

42 W. C. Claycomb, N. A. Lanson, Jr., B. S. Stallworth, D. B. Egeland, J. B. Delcarpio, A. Bahinski and N. J. Izzo, Jr., *Proc. Natl. Acad. Sci. U. S. A.*, 1998, **95**, 2979-2984.

43 43. Y. Leverrier and A. J. Ridley, *Nat. Cell Biol.*, 2001, **3**, E91-93.

44 M. L. Coleman, E. A. Sahai, M. Yeo, M. Bosch, A. Dewar and M. F. Olson, *Nat. Cell Biol.*, 2001, **3**, 339-345.

45 J. C. Mills, N. L. Stone, J. Erhardt and R. N. Pittman, *J. Cell Biol.*, 1998, **140**, 627-636.

46 C. Lu, P. Li, R. Gallegos, V. Uttamsingh, C. Q. Xia, G. T. Miwa, S. K. Balani and L. S. Gan, *Drug Metab. Dispos.*, 2006, **34**, 1600-1605.

47 H. Liu, C. Sabus, G. Carter, C. Du, A. Avdeef and M. Tischler, *Pharm. Res.*, 2003, **20**, 1820-1826.

48 E. H. Kerns, L. Di, S. Petusky, M. Farris, R. Ley and P. Jupp, *J. Pharm. Sci.*, 2004, **93**, 1440-1453.

49 A. Avdeef, S. Bendels, L. Di, B. Faller, M. Kansy, K. Sugano and Y. Yamauchi, *J. Pharm. Sci.*, 2007, **96**, 2893-2909.

50 Y. H. Ahn, Y. Hwang, H. Liu, X. J. Wang, Y. Zhang, K. K. Stephenson, T. N. Boronina, R. N. Cole, A. T. Dinkova-Kostova, P. Talalay and P. A. Cole, *Proc. Natl. Acad. Sci. U. S. A.*, 2010, **107**, 9590-9595.

51 K. Taguchi, H. Motohashi and M. Yamamoto, *Genes Cells*, 2011, **16**, 123-140.

52 A. T. Dinkova-Kostova, W. D. Holtzclaw, R. N. Cole, K. Itoh, N. Wakabayashi, Y. Katoh, M. Yamamoto and P. Talalay, *Proc. Natl. Acad. Sci. U. S. A.*, 2002, **99**, 11908-11913.

53 T. S. Chong, P. Li, W. K. Leong and W. Y. Fan, *J. Organomet. Chem.*, 2005, **690**, 4132-4138.

54 G.-Y. Liou and P. Storz, *Free Radical Res.*, 2010, **44**, 479-496.

55 P. T. Schumacker, *Cancer Cell*, **10**, 175-176.

56 M. Valko, C. J. Rhodes, J. Moncol, M. Izakovic and M. Mazur, *Chem.-Biol. Interact.*, 2006, **160**, 1-40.

57 D. Trachootham, J. Alexandre and P. Huang, *Nat Rev Drug Discov*, 2009, **8**, 579-591.

58 I. Vermes, C. Haanen, H. Steffens-Nakken and C. Reutelingsperger, *J. Immunol. Methods*, 1995, **184**, 39-51.

Graphical Abstract

$CpFe(CO)_2$ complexes kill cancer cells while leaving normal cells unharmed.